Induced Micro Variations in Hydrodynamic Bearings

Charles Baroud, Ilene Busch-Vishniac, and Kristin Wood

Department of Mechanical Engineering

The University of Texas MC C2200

Austin, TX 78712-1043

June 22, 1999

Abstract

Fluid-Structure interactions in hydrodynamic bearings result in load carrying and drag forces which give the bearing its characteristics. While these bearings offer many benefits as machine components, one of their shortcomings is their limited efficient range. In this paper, we demonstrate the use of micron-scale actuators to actively control the lift and drag forces on a slider bearing. We show that for a set of control parameters, we are able to affect the performance of a bearing by more than 100% during operation, increasing the bearing's range of operation.

1 Introduction

The field of microelectromechanical systems (MEMS) has shown great promise in the last 20 years with the emergence of new manufacturing techniques. Nevertheless, these MEMS devices are not widely available in applications. Even though the idea of acting on the

environment at such a scale seems quite attractive, useful applications have been slow in developing.

Many uses for MEMS have been suggested in fluid dynamical systems, both as actuators and as sensors as reviewed in Ho and Tai (1996) Ho and Tai (1998). For example, they suggest using MEMS elements as pressure sensors or controllers in fluidic systems. Part of the aesthetic appeal of fluid applications of MEMS comes from the continuum nature of fluids, even at scales which are very small compared to everyday applications. One can imagine channels, orifices, valves, or pistons to act similarly at both micron and millimeter scales, provided the Reynolds numbers are similar. [1]

In this paper, we study the application of MEMS in hydrodynamic bearings, where the goal is to adapt the bearings to changes in their operating environment. While hydrodynamic bearings (e.g. journal, slider and thrust bearings) work quite well in the range of parameters for which they are designed, they do not respond very well to changes in the operating conditions. This problem is most evident in rotating machines at startup, shut-down and resonant frequencies, but it can also be important when variations in rotation rate are required. Therefore, one would like to design a bearing that can sense its environment and adapt itself to it.

Surface roughess has a significant influence on the behavior of a thin film bearing (Christensen (1970)). This roughness can take the form of grooves and/or "bumps" with characteristic separations small compared to the scale of the system. The effect of surface roughness is different for different geometries, as discussed for example by Hargreaves (1991) and Gururajan and Prakash (1999). We can therefore imagine integrating an array of sensors and actuators into the bearing surface which would evaluate the local

[1] The assumption here is that other forces, such as electro-static or molecular forces, are negligible.

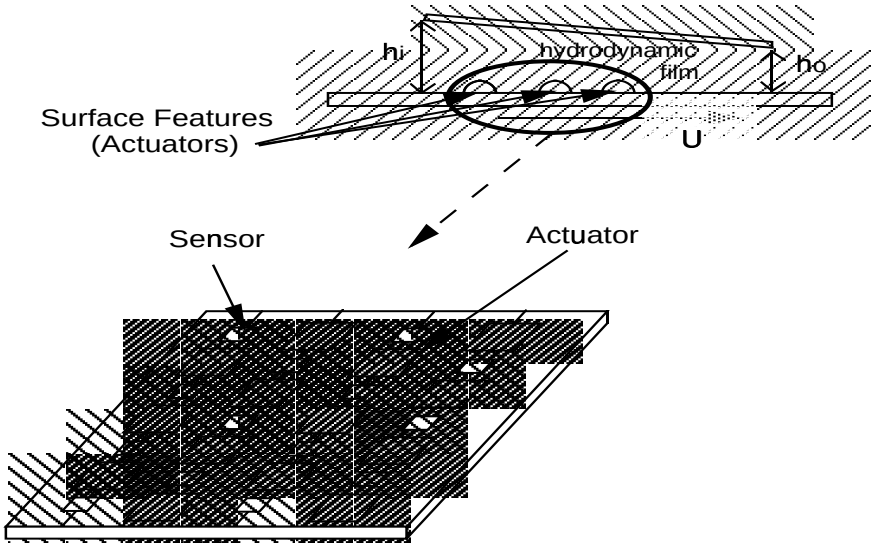

Figure 1: Schematic of novel MEMS array.

environmental conditions and adapt the surface shape accordingly (see Fig. 1).

Previous experiments studied the feasibility of such a system from a design point of view (Koeneman (1995); Koeneman et al. (1997)). At the same time, Flagg (1995), Masser (1995), Maddox (1994), Chu et al. (1998), and Wood et al. (1998) characterized the effect of rough surfaces on the behavior of a slider bearing. Their work and the basic experimental apparatus are described in the next section. In this paper, we significantly extend the previous work by changing the bearing surface characteristics dynamically while in operation. The experiments are described in Sec. 3 and the results are given in Sec. 4.

2 Experimental Apparatus and Previous Work

The apparatus used in this study is shown in Fig. 2. It consists of a modified grinder where the grinding wheel is replaced with a smooth steel disk. To this grinder, a specially

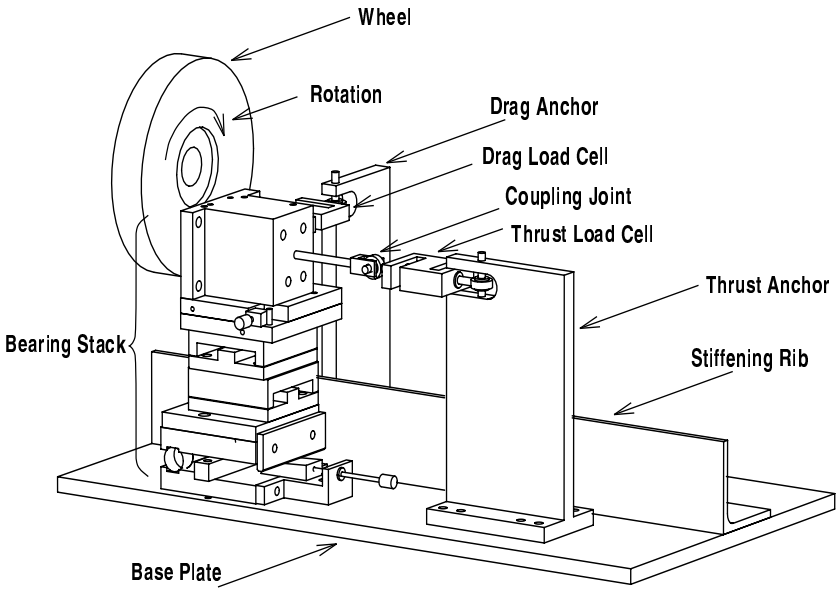

Figure 2: Bearing experimental assembly.

manufactured "bearing stack" can be attached. This assembly holds a manifold that simulates a bearing pad (at actual one-to-one gap scales) as well as displacement eddy current sensors which measure the distance between the pad and the wheel. Attached to the stack are two load cells that measure the forces parallel and perpendicular to the wheel. The force measurements can be used simply to characterize the bearing performance over time.

A nozzle drives a jet of synthetic oil (ISO 45) between the steel wheel and the bearing manifold as the two surfaces are held between $75\mu m$ and $100\mu m$ apart. Since the surfaces are not parallel, the fluid pressure rises within the gap, thus generating a thrust force.

In Masser's (1995) experiments, the surface of the manifold was made up of one of three masks, each with different surface shape characteristics. The three masks were etched in silicon. The first was completely smooth whereas the two others had grooves,

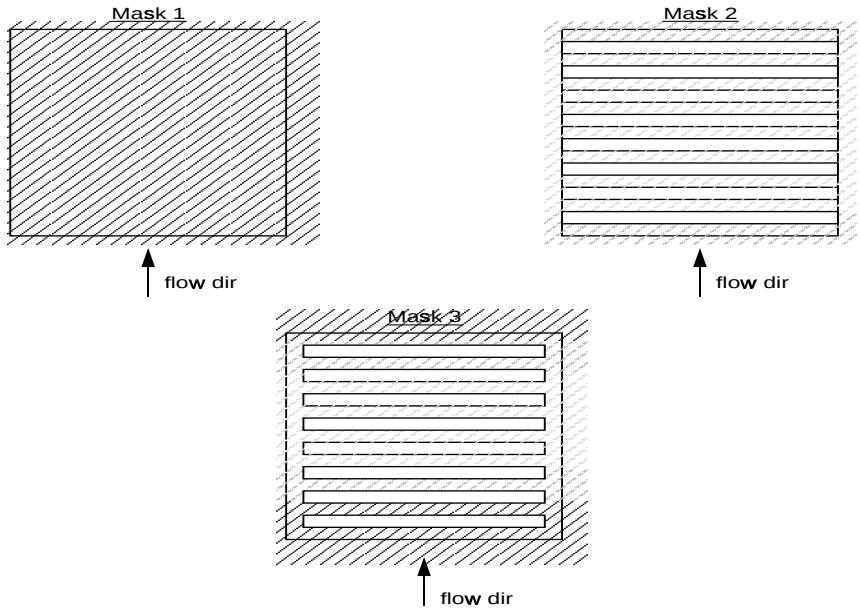

Figure 3: Masks used in previous experiments. Mask 1 is flat, while masks 2 and 3 have $50\mu m$ grooves etched in them, extending all the way across only in mask 2.

$50\mu m$ deep etched into them as shown in Fig. 3. He found that the behavior depended on the mask as shown in Fig. 4.

Using the experimental apparatus shown in Fig. 2, Masser (1995) tested a number of bearing surfaces, with the objective to match within the experimental certainty the results predicted by Maddox (1994). For example, Fig. 4 shows the experimental results obtained for a flat silicon surface and a fixed featured surface at a constant taper angle. The trends shown in the figure match the trends of the computational results. These data also indicate that loads can be varied significantly for featured bearing surfaces and for different feature lengths. For a detailed discussion of the results obtained previously, the reader is referred to Wood et al. (1998).

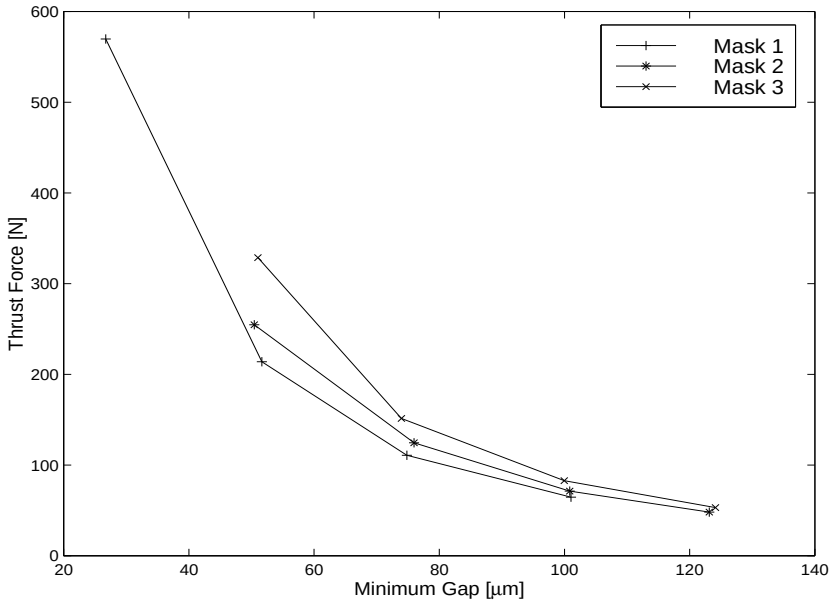

Figure 4: Experimental results of thrust load versus film thickness: fixed surface features on a experimental slider bearing. From Masser (1995).

3 Current Experiment: Deformable Surface Features

In the current experiment, the silicon masks are replaced with aluminum equivalents where the grooves penetrate all the way through the mask thickness. The new masks are 2.54cm squares and the grooves extend 2.3cm across them. These whole surface is then covered with adhesive tape ($25\mu m$ thick). By applying pressure behind the masks from a nitrogen cylinder, the tape is deformed, thus changing the "roughness" (shape) of the surface while the bearing is running. Figure 5 shows a schematic of the tape deformation under pressure. Even though the exact shape of the tape is not controlled during a run, we are able to characterize the behavior of the bearing with respect to the drive pressure.

Some tests were performed under a confocal microscope to estimate the deformation of the tape due to the driving pressure. Even though the actual shape of the deformed

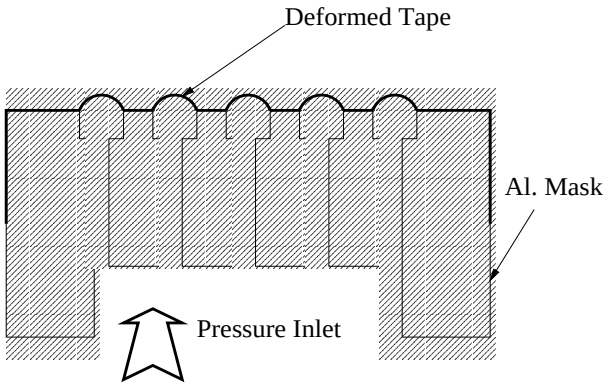

Figure 5: Schematic cut through the mask showing the tape deformation under pressure.

tape will be different in the experiment, these tests give us an estimate of the amount of deformation to be expected. In reality, the lateral forces from the oil flow, as well as the interactions between the driving pressure and the pressure of the flow make the problem quite complicated. However, as an order of magnitude estimate, we found that for the pressure differences predicted by Maddox (1994), the tape deformation is expected to vary between 10 and $50\mu m$.

The experimental procedure was implemented using a factorial design technique. Using the previous experiments as reference, we chose to study the effects of the following parameters:

- The minimum gap (x_1) separating the two surfaces: 75 and $100\mu m$.
- The relative orientation of the two surfaces, characterized by the ratio (x_2) of the two distances at the leading and trailing edges. The two ratios were 1.5 and 2.0.
- The driving pressure deforming the tape (x_3): the values were 0, 3.10×10^5 and 5.17×10^5 Pascals.
- The width (x_4) of the grooves in the masks: $80\mu m$ and $50\mu m$.

x_1	X_{min}	[-1, 1]
		[$75\mu m$, $100\mu m$]
x_2	H_x	[-1, 1]
		[2.0, 1.5]
x_3	Pressure	[-1, 0, 1]
		[0psi, 3.1e5Pa, 5.2e5Pa]
x_4	Mask	[-1, 1]
		[mask1, mask2]

Table 1: The variables and their values.

These variables are also shown in Table 1. The top line for each variable gives the normalized value (which will be used below in the phenomenological model) while the value below gives the actual physical value.

A total of 24 experiments are run to study the effect of varying each of the parameters on the thrust and drag forces. The experiments are run in random order so as to remove any bias introduced by the experimental setup. Finally, replicates of the experiments are also run to determine the overall magnitude of the experimental error. This experimental design method is well documented in the works of Box and Draper (1987) and DeVor et al. (1992).

4 Experimental Results

By taking the force at zero drive pressure as the reference, we could measure the change in the forces as the pressure was applied behind the bearing. The difference in the forces for both "drag" and "thrust" was measured for both masks, in accordance with the experimental design. The two masks differ only by the width of their grooves.

The initial forces were also measured; the initial thrust force varied between about 45N and 110N, while the drag force was in the range 4.5N to 10N. However, the absolute value for intial force was less repeatable than the change that was measured as the pressure was

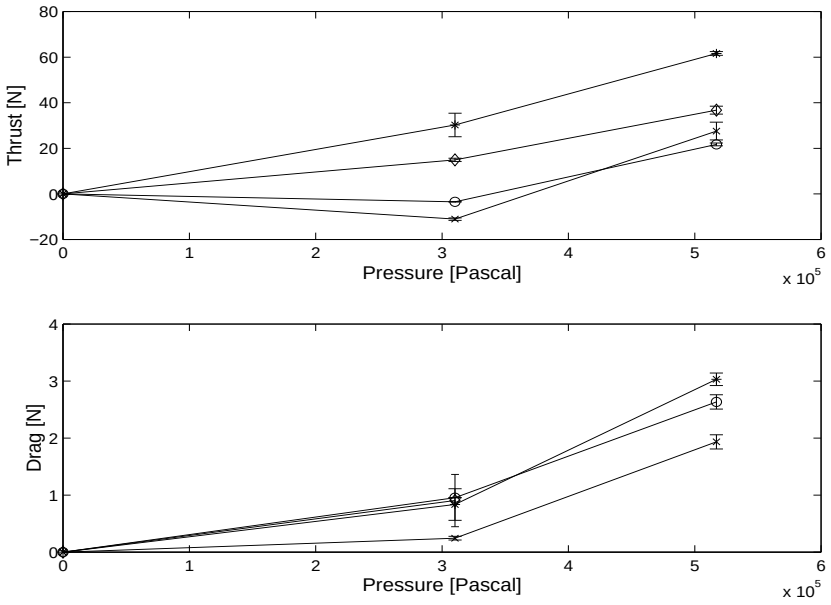

Figure 6: The thrust and drag differentials for mask 1. the '**x**' corresponds to the case when $X_{min} = 75\mu m$ and $H_x = 2.0$. '**o**' corresponds to $X_{min} = 100\mu m$ and $H_x = 2.0$. '+' corresponds to $X_{min} = 75\mu m$ and $H_x = 1.5$. '*' corresponds to $X_{min} = 100\mu m$ and $H_x = 1.5$.

applied.

The test results are plotted in Figs. 6 And 7. The pressure is shown on the x-axis, while the y-axis shows the change in thrust and drag forces. This arrangement leaves us with four combinations of x_1 and x_2 for each mask. The drag value for mask 1 (6) is treated as an outlier and its value is not shown, since we were unable to re-take the data point..

The data for the first mask are plotted in Fig. 6, and the data for mask 2 are plotted in Fig. 7. These results are described below.

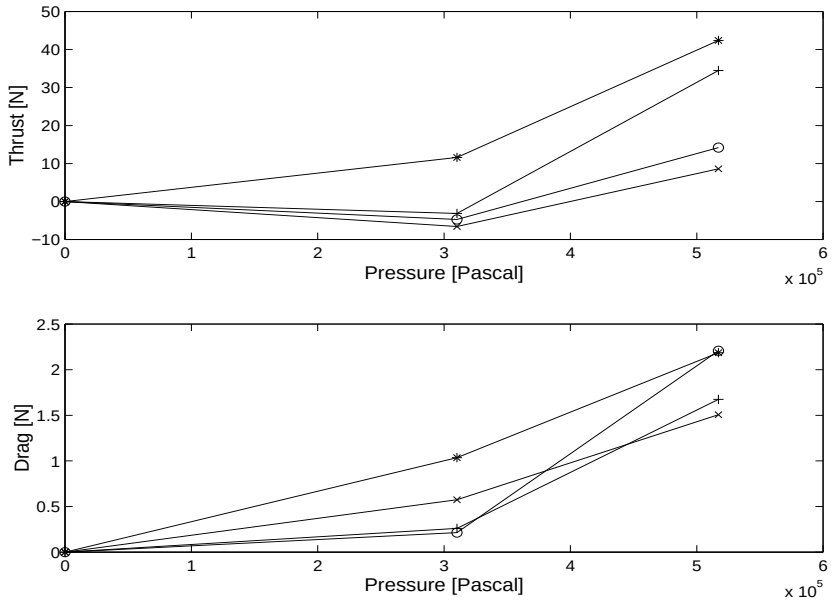

Figure 7: The thrust and drag differentials for mask 2

4.1 The thrust force

The thrust force measurements were found to be much more repeatable (and therefore more meaningful) than the drag force measurements. The reason for this result was that the level of the thrust force was well into the useful range of the instruments, while that of the drag force was relatively low.

For both masks, the thrust force was found to have the following pattern:[2]

- At 5.17×10^5 Pa, the force was invariably higher than it was with no driving pressure. The increase was between 10 and 60 N, or between 20% and 120% from the force with zero pressure, for the first mask, and 10% and 60% for the second one. Typically, larger changes are found in the cases where the initial forces are the lowest.

[2]Note that the force with no driving pressure was identically set to zero, since we are interested in its variations only.

- At 3.10×10^5 Pa, we measured either a small decrease in the force, or a small increase; the changes for the most part stayed within 20% of the forces at zero pressure.

4.2 The drag force

The drag forces experienced by the bearing runner also followed a distinct pattern:

- At 5.17×10^5 Pa, the drag force gained about 1.5 - 3 N, or between 20% and 50% from its value with no driving pressure.
- At 3.10×10^5 Pa, the drag force also showed a steady increase, by about 0.2-1 N, or between about 5% and 10%.

5 Phenomenological Model and Discussion

By taking the results of the experiments shown above, we applied an Analysis of Variants (ANOVA) method in order to derive a phenomenological model of the system (Ross (1996) and Baroud (1997)). The ANOVA method not only provides us with an expression which best fits the data, but it also gives a way to determine which of the measured quantities are significant compared to the measurement uncertainties. Only the measurements above the noise level are retained in the final expression. In this technique, each of the above variables is given the -1 or $+1$ depending on whether it is high or low (except for the pressure which can also take on the value zero at 3.10×10^5Pa). The final model can then guide us as to which effects most significantly alter the physics.

The small experimental error came mainly from the instrumentation, such as the uncertainty in the measured forces, pressures, or distances. Furthermore, the force readings had to be made soon after the pressure was applied to avoid the effects of plastic deformation of the tape. Table 2 shows the uncertainty in each of the measurements, as

Variable	Absolute variation	Percent variation
X_{min}	$\pm 2\mu m$	2%
H_x	± 0.08	4%
Pressure	$< \pm 35 KPa$	7%

Table 2: Estimated uncertainty in the measurements. Figures are based on the repeated runs and are used in the ANOVA to determine the validity of the model.

estimated from the repetition of the runs. However, the ANOVA method allows us to estimate the uncertainty in our data in a more analytical way. By comparing the results obtained for two separate trials, we can set a cutoff which depends on the repeatability of the measurements.

We simplify the numerical model by sub-dividing the results for the two different masks into two separate equations for y^1 and y^2, respectively. We are then left with four equations of three variables (two for thrust and two for drag force). These equations are more informative than the complete four variable model.

For the thrust force, the model is shown in Eq. 1.

$$\begin{aligned} y_t^1 &= 6.55 + 13.82x_1 + 18.17x_3 + 11.62{x_3}^2 + 6.67x_1x_3 - 7.16x_1{x_3}^2 \\ y_t^2 &= -0.702 + 4.936x_1 + 12.462x_3 + 13.16{x_3}^2 + 6.76x_1x_3 \end{aligned} \tag{1}$$

In the above equation, it is clear that the driving pressure (x_3) is the most important factor, since both the x_3 and the x_3^2 terms have large multiplicative constants (coefficients) before them. This result supports our claim that the deformation of the tape – which is closely related to the driving pressure – is a very important factor in the thrust force of the bearing. Other important factors are the distance (x_1) and the interaction between the distance and the deformation. These observations are reasonable since the deformation

of the membrane changes the effective distance between the runner and the pad. These observations hold true for both masks, to within reasonable uncertainty in the coefficients.

The model for the drag force is shown in Eq. 2.

$$\begin{aligned} y_d^1 &= 0.744 + 1.132x_3 + 0.389{x_3}^2 + 0.284x_2x_3 + 0.265x_1x_2x_3^2 \\ y_d^2 &= 0.522 + 0.947x_3 + 0.425{x_3}^2 + 0.284x_1x_2 + 0.151x_2x_3 - 0.307x_1x_2x_3^2 \end{aligned} \tag{2}$$

In these equations, the driving pressure terms x_3 and x_3^2 are still found to be very important in affecting the drag force. The coefficient of x_3 is as much as an order of magnitude larger than some of the other coefficients, which means that this term has the greatest effect on the data. However, the relatively low importance of x_1 (which only appears in interaction terms) also makes the terms in $x_1 \cdot x_3^i$ less important.

Furthermore, it is interesting to note the presence of the cross terms x_2x_3, And, to a less important degree, $x_2x_3^2$. While x_3 represents the deformation of the membrane, x_2 correlates the "effective surface area" that is seen by the fluid. The cross terms then signify that the two quantities interact to increase the drag.

6 Discussion, Conclusions, and Future Directions

Geometric design parameters have an effect on the performance of hydrodynamic bearing systems. These variations in geometric form could be accommodated through macroscopic or microscopic methods of actuation and sensory control. This research effort explores the possibility of implementing microscopic devices in the role of sensors and actuators. The choice of micro over macro is based upon the recent advancements of VLSI manufacturing technology – which have also lead to the sudden proliferation of integrable

microelectromechanical devices. Such an integrated system could reduce or eliminate the need for external actuator and sensory devices. This advantage saves space and required power, while increasing the possibilities of local fluid control.

Because of the potential advantages of local surface control, this research concentrates on creating microscale surface deformations on slider bearing surfaces to produce macroscale performance variations. The ability to actively deform bearing surfaces will allow for the design of bearings which may control one or more of the following performance characteristics: stiffness, damping, load capacity, power loss, cavitation, film thickness, clearance, etc.

A specific experiment is considered in this paper: the effect of deformable shapes on the bearing surfaces. Aluminum bearing plates with pressure actuated tape membranes provide the media for carrying out the experiment. Although not directly measured during the runs, we estimate that the tape deformation during the experiment was on the order of 10 to $50\mu m$. Therefore, we can deduce, from the experimental results, that for such small deformations in the surface of a bearing, we can expect to affect its performance significantly. This result is what we set out to show in the project, thus giving us confidence in further pursuing the idea of embedding MEMS into the surface of hydrodynamic bearings.

Future work, however, should consider the surface deformations directly and relate the changes in the forces directly to a particular geometric feature. Furthermore, one would want to understand the difference in forces between grooves and bumps, in order to better design the features and build actual structures in silicon or other materials. Based on such extensions, fully integrated systems may be advanced for hydrodynamic bearings. Analogous applications may also be considered, such as self-adjusting seals in centrifugal pumps and other rotating machinery.

7 Nomenclature

- X_min : Minimum distance separating two surfaces.
- H_x : Ratio of distance at leading edge over trailing edge.
- x_1 : Normalized X_min.
- x_2 : Normalized H_x.
- x_3 : Normalized drive pressure.
- x_4 : Mask descriptor.
- y_t^1 : Thrust force for mask 1.
- y_t^2 : Thrust force for mask 2.
- y_d^1 : Drag force for mask 1.
- y_d^2 : Drag force for mask 2.

References

Baroud, C. N., 1997, "Induced Dynamical Variations in Hydrodynamic Bearings," Master's thesis, The University of Texas at Austin, Austin, Texas.

Box, G., Draper, N., 1987, *Empirical Model-Building and Response Surfaces* John Wiley and Sons.

Christensen, H., 1970, "Stochasatic Model for Hydrodynamic Lubrication of Rough Surfaces," *Proc. Instn. Mech. Engrs.*, Vol. 184, pp. 1013.

Chu, C. S., Wood, K. L., Busch-Vishniac, I., 1998, "Nonlinear Dynamic Modeling with Confidence Bounds of Hydrodynamic Bearings," *ASME Journal of Tribology*, Vol. 120, pp. 595–604.

DeVor, R. E., Chang, T., Sutherland, J. W., 1992, *Statistical Quality Design and Control: Contemporary Concepts and Methods* Macmillan Publishing Company, New York.

Flagg, S. W., 1995, "Design and Construction of an Apparatus to Test Active Hydrodynamic Bearings," Master's thesis, The University of Texas at Austin, Austin, Texas.

Gururajan, K., Prakash, J., 1999, "Surface Roughness Effects in Infinitely Long Porous Journal Bearings," *ASME Journal of Tribology*, Vol. 121, pp. 139–147.

Hargreaves, D., 1991, "Surface waviness effects on the load-carrying capacity of rectangular slider bearings," *Wear*, Vol. 145, pp. 137–151.

Ho, C.-M., Tai, Y.-C., 1996, "Review: MEMS and Its Applications for Flow Control," *Journal of Fluids Engineering*, Vol. 118, pp. 437–446.

Ho, C.-M., Tai, Y.-C., 1998, "Micro-Electro-Mechanical-Systems (MEMS) and Fluid Flows," *Annual Review of Fluid Dynamics*, Vol. 30, pp. 579–612.

Koeneman, P., Busch-Vishniac, I., Wood, K., 1997, "Feasibility of MEMS Micro Power Supplies," *IEEE Journal of Microelectromechanical Systems*, Vol. 6, pp. 355–362.

Koeneman, P. B., 1995, "Conceptual Design of a Micro Power Supply for a MEMS Smart Bearing," Master's thesis, The University of Texas at Austin, Austin, Texas.

Maddox, W. E., 1994, "Modeling and Design of a Smart Hydrodynamic Bearing with an Actively Deformable Surface," Master's thesis, The University of Texas at Austin, Austin, Texas.

Masser, D. I., 1995, "An Experimental Investigation of Hydrodynamic Bearings with Micromachined Surfaces.," Master's thesis, The University of Texas at Austin, Austin, Texas.

Ross, P. J., 1996, *Taguchi Techniques for Quality Engineering* McGraw Hill, New York.

Wood, K., Neikirk, D. et al., 1998, "MEMs Hydrodynamic Bearings: Applications and Implications to Machine Failure Prevention," *Journal of Tribotest*, Vol. 4, pp. 275–288.